iScience, Volume *26*

Supplemental information

LINC00116-encoded microprotein mitoregulin regulates fatty acid metabolism at the mitochondrial outer membrane

Shan Zhang, Yabo Guo, Gio Fidelito, David R.L. Robinson, Chao Liang, Radiance Lim, Zoë Bichler, Ruiyang Guo, Gaoqi Wu, He Xu, Quan D. Zhou, Brijesh K. Singh, Paul Yen, Dennis Kappei, David A. Stroud, and Lena Ho

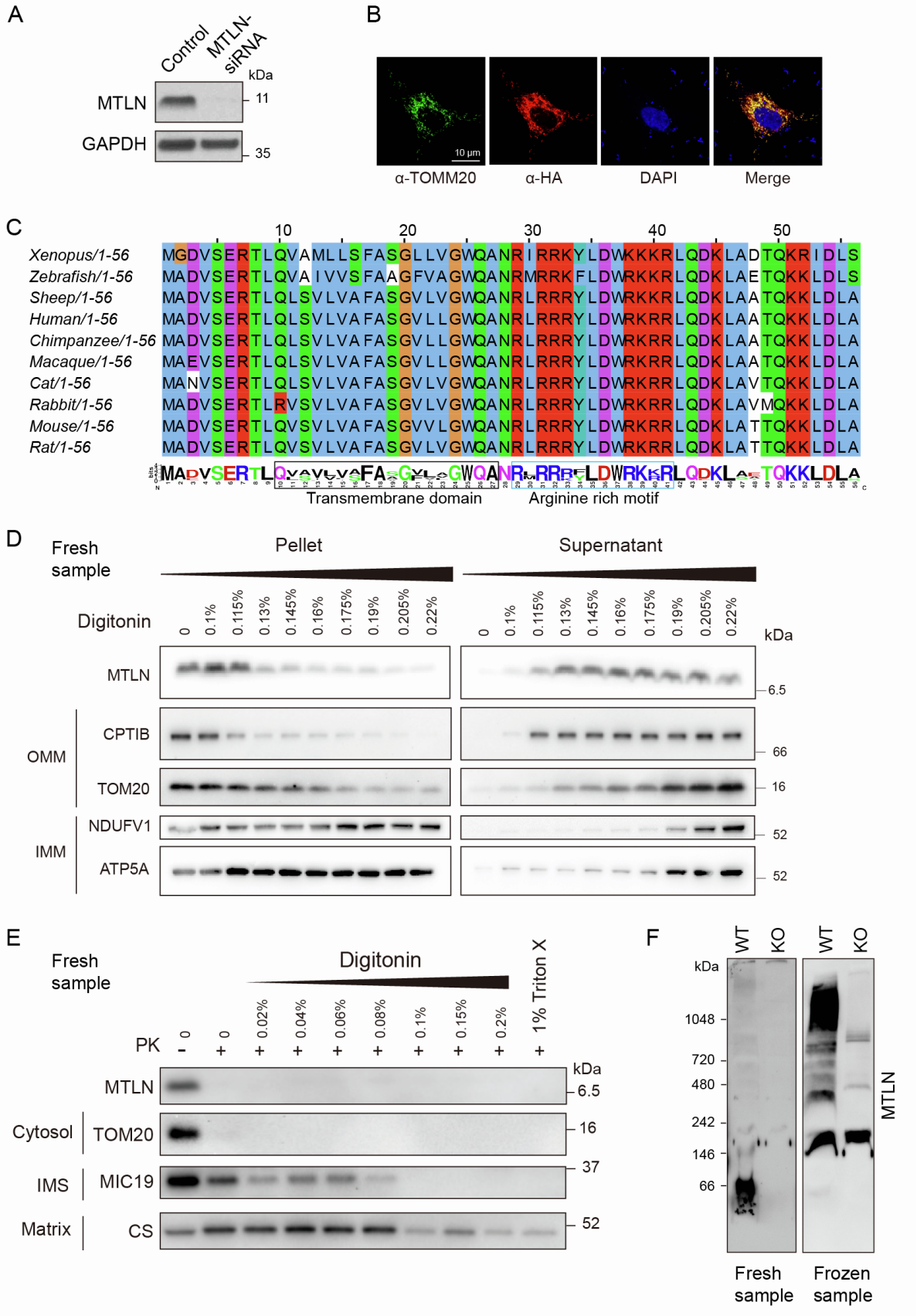
A
Control
MTLN-siRNA
kDa
MTLN
11
GAPDH
35
B
10 μm
α-TOMM20
α-HA
DAPI
Merge
C
Xenopus/1-56
Zebrafish/1-56
Sheep/1-56
Human/1-56
Chimpanzee/1-56
Macaque/1-56
Cat/1-56
Rabbit/1-56
Mouse/1-56
Rat/1-56
Transmembrane domain
Arginine rich motif
D
Fresh sample
Pellet
Supernatant
Digitonin
0
0.1%
0.115%
0.13%
0.145%
0.16%
0.175%
0.19%
0.205%
0.22%
kDa
MTLN
6.5
OMM
CPTIB
66
TOM20
16
IMM
NDUFV1
52
ATP5A
52
E
Fresh sample
Digitonin
PK
1% Triton X
kDa
MTLN
6.5
Cytosol
TOM20
16
IMS
MIC19
37
Matrix
CS
52
F
WT
KO
WT
KO
kDa
1048
720
480
242
146
66
MTLN
Fresh sample
Frozen sample

Figure S1. Microprotein MTLN is localized to the outer membrane of mitochondria, Related to Figure 1.

(A) Knock-down of MTLN in U2OS cells by siRNA.

(B) Co-immunostaining of HA tagged MTLN with mitochondrial marker TOMM20 in HeLa cell.

(C) Sequence alignment of MTLN homologs. Positions of the transmembrane domain and the arginine rich motif are indicated.

(D) Solubilization of mitochondrial proteins isolated from freshly dissected mouse skeletal muscle by a gradient of digitonin.

(E) Protease sensitivity assay of mitochondrial proteins isolated from freshly harvested C2C12 myoblast.

(F) Mobility of MTLN analysed by native-PAGE in mitochondria isolated from freshly dissected and frozen mouse skeletal muscle. Mitochondria were solubilized for native-PAGE right after the isolation.

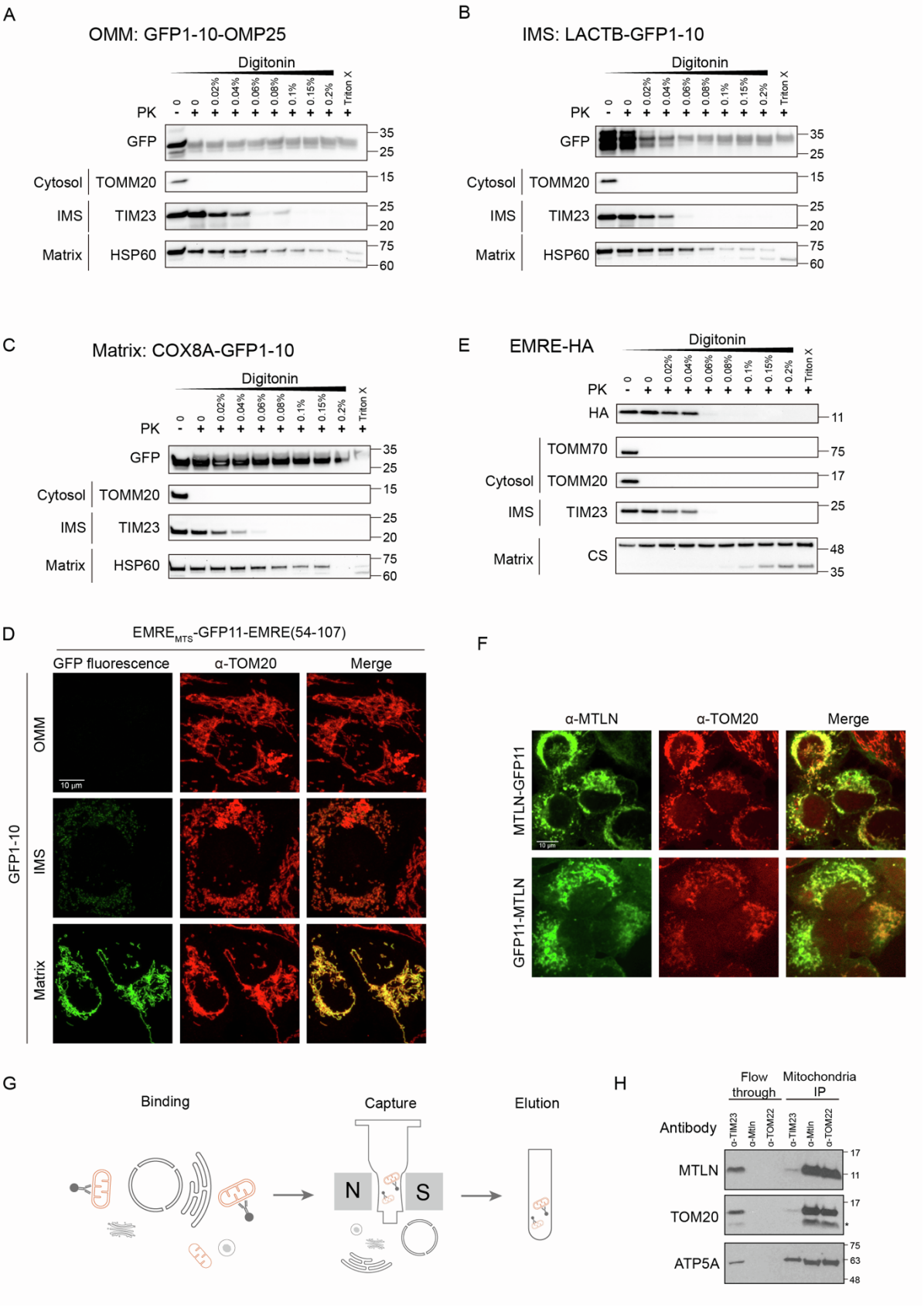
A
OMM: GFP1-10-OMP25
Digitonin
PK
GFP
Cytosol
TOMM20
IMS
TIM23
Matrix
HSP60
B
IMS: LACTB-GFP1-10
C
Matrix: COX8A-GFP1-10
D
EMRE$_{MTS}$-GFP11-EMRE(54-107)
GFP fluorescence
α-TOM20
Merge
GFP1-10
OMM
IMS
Matrix
10 μm
E
EMRE-HA
HA
TOMM70
CS
F
α-MTLN
MTLN-GFP11
GFP11-MTLN
G
Binding
Capture
Elution
N
S
H
Flow through
Mitochondria IP
Antibody
α-TIM23
α-Mtln
α-TOM22
MTLN
TOM20
ATP5A

Figure S2. In vivo protein topology analysis confirms the OMM localization of MTLN, Related to Figure 2.

(A) Protease sensitivity assay of OMM GFP1-10 (GFP1-10-OMP25). TOM20, TIM23, and HSP60 are markers of cytosolic side of OMM, IMS, and matrix, respectively. A small fraction of GFP1-10 remained resistant to protease under fully solubilization of membrane by Triton X. This set of experiments were done using HEK293T cells transfected with GFP1-10 constructs. Mitochondria were isolated from freshly harvested cells and used for the assay.

(B) Protease sensitivity assay of IMS GFP1-10: LACTB-GFP1-10.

(C) Protease sensitivity assay of matrix GFP1-10: COX8A-GFP1-10.

(D) Representative GFP fluorescence and TOM20 staining signals of HEK293T cells co-transfected with $EMRE_{MTS}$-GFP11-EMRE(54-107) and OMM, IMS, and matrix GFP1-10.

(E) Protease sensitivity assay of EMRE-HA.

(F) Immunostaining of MTLN and TOM20 in HEK293T cells transfected with GFP11-MTLN and MTLN-GFP11 constructs.

(G) Schematic diagram for antibody-based mitochondria purification.

(H) MTLN antibody purified mitochondria as efficient as the TOM22 antibody. Cytosolic homogenate of wild type HEK293T cell was incubated with magnetic protein A beads coated with indicated antibodies. TOM20 and ATP5A are markers OMM and IMM, respectively.

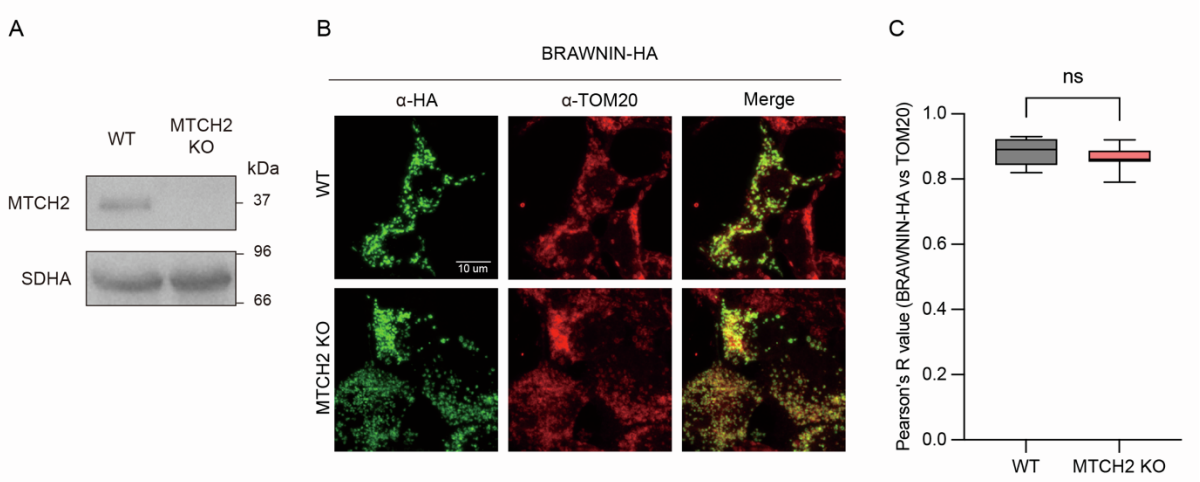

Figure S3. Mitochondrial targeting of MTLN is impaired by the deficiency of OMM α-helical protein insertase, Related to Figure 3.

(A) Western validation of the MTCH2 KO HEK293T cell generated by CRISPR-Cas9 based gene editing.

(B) Immunostaining of HA and TOM20 in WT and MTCH2 KO HEK293T cells transfected with the IMM α-helical protein BRAWNIN-HA.

(C) Quantitative analysis of mitochondrial localization of BRAWNIN-HA in WT and MTCH2 KO HEK293T cells. Pearson's correlated values between HA and TOM20 signals were calculated for individual cells using ImageJ and plotted. Error bars of the box plot shows the minimum and maximum values with boxes extend from the 25th to 75th percentiles, and the *p*-value was calculated by unpaired t-test.

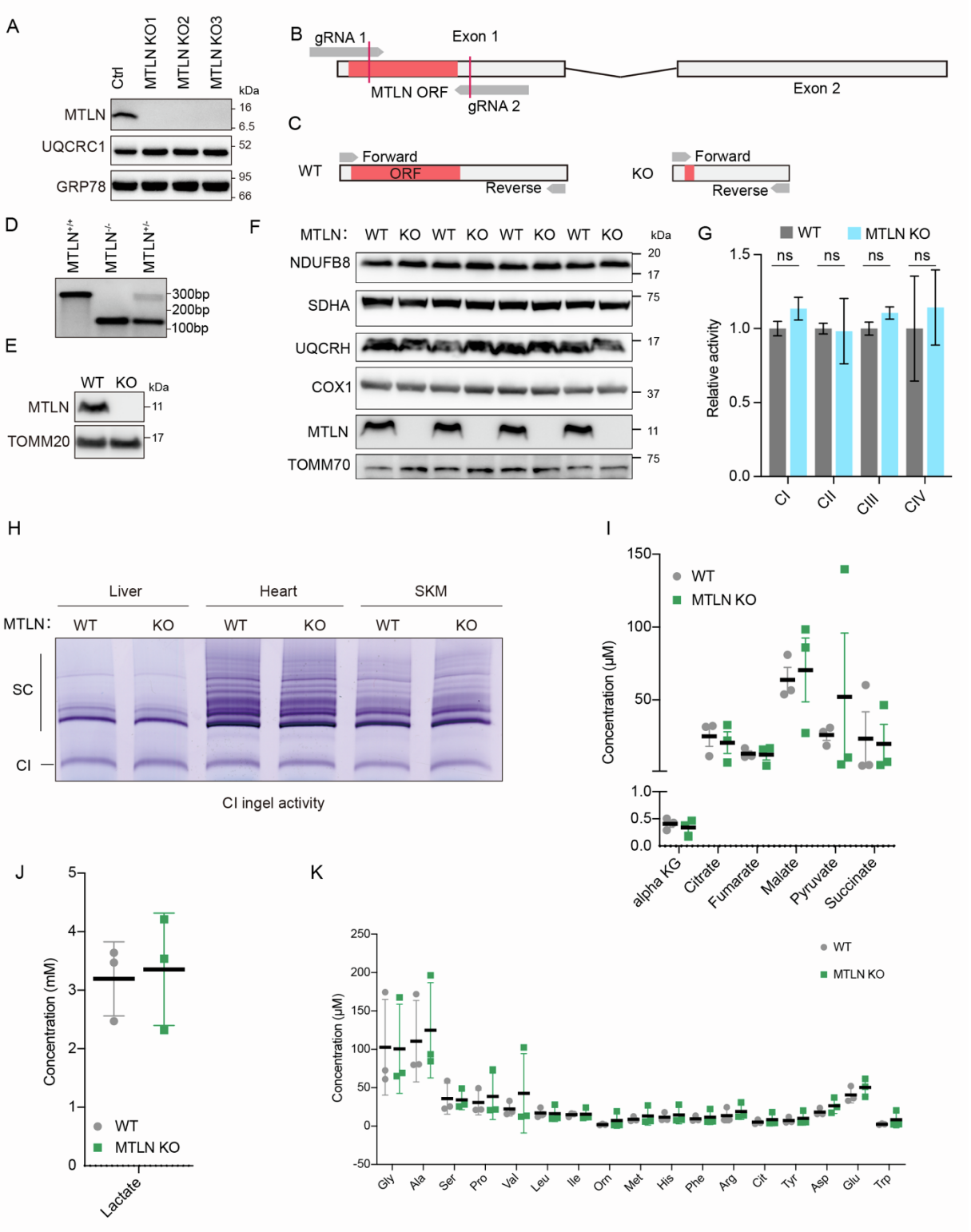

Figure S4. Loss of MTLN does not impair mitochondrial respiratory chain, Related to Figure 4.

(A) Validation of MTLN KO C2C12 cell lines by immunoblotting.

(B) Design of gRNAs in the generation of MTLN global KO in mouse.

(C) Schematic diagram of the mouse genotyping strategy.

(D) Validation of MTLN KO in mouse by PCR.

(E) Validation of MTLN KO in mouse heart by protein immunoblotting.

(F) Western analysis of respiratory chain subunits in heart mitochondria of WT and MTLN KO mice. NDUFA8, SDHA, UQCRH, and COX1 are subunits of respiratory chain complex I-IV, respectively.

(G) Enzymatic activities of respiratory chain complexes measured using heart mitochondria of WT and MTLN KO mice. Mean and SEM of four biological replicates are shown, p-values were calculated from two-sided, unpaired t-test.

(H) A zoom-in view of the complex I in gel assay shown in Fig. 4B. Positions of complex I (CI) and supercomplexes (SC) are denoted.

(I) Abundance of organic acids measured by mass spectrometry in mouse skeletal muscles.

(J) Similar to (I), lactate was measured.

(K) Similar to (I), amino acids were measured.

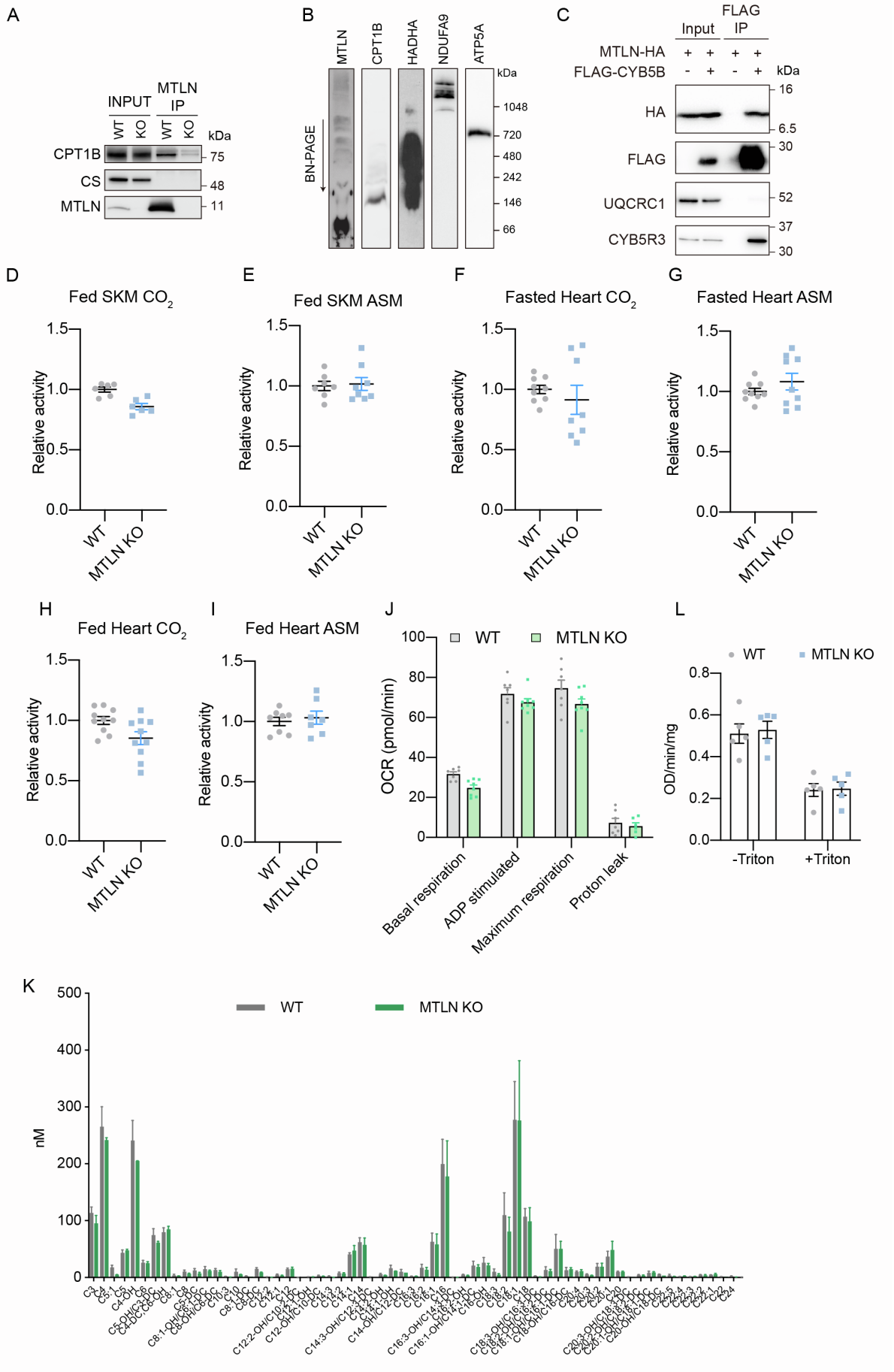
A
INPUT
MTLN IP
WT
KO
WT
KO
kDa
CPT1B
75
CS
48
MTLN
11
B
MTLN
CPT1B
HADHA
NDUFA9
ATP5A
kDa
BN-PAGE
1048
720
480
242
146
66
C
FLAG
Input
IP
MTLN-HA
FLAG-CYB5B
kDa
HA
16
6.5
FLAG
30
UQCRC1
52
CYB5R3
37
30
D
Fed SKM CO2
E
Fed SKM ASM
F
Fasted Heart CO2
G
Fasted Heart ASM
Relative activity
1.5
1.0
0.5
0.0
WT
MTLN KO
H
Fed Heart CO2
I
Fed Heart ASM
J
WT
MTLN KO
OCR (pmol/min)
100
80
60
40
20
0
Basal respiration
ADP stimulated
Maximum respiration
Proton leak
L
WT
MTLN KO
OD/min/mg
0.8
0.6
0.4
0.2
0.0
-Triton
+Triton
K
WT
MTLN KO
nM
500
400
300
200
100
0
C3
C4
C5:1
C5
C4-OH
C5-OH/C3-DC
C4-DC/C6-OH
C6
C8:1
C8
C5:1-DC
C6-DC
C8:1-OH/C6:1-DC
C8-OH/C6-DC
C10:3
C10:2
C10
C8:1-DC
C8-DC
C12:2
C12:1
C12
C12:2-OH/C10:1-DC
C12-OH/C10-DC
C14:3
C14:2
C14:1
C14:3-OH/C12:1-DC
C14:2-OH/C12:1-DC
C14-OH/C12-DC
C16:3
C16:2
C16:1
C16:3-OH/C14:1-DC
C16:2-OH/C14:1-DC
C16:1-OH/C14-DC
C16-OH
C18:3
C18:2
C18:1
C18:3-OH/C16:1-DC
C18:2-OH/C16:1-DC
C18:1-OH/C16-DC
C18-OH/C16-DC
C20:4
C20:3
C20:2
C20:1
C20
C20:3-OH/C18:1-DC
C20:2-OH/C18:1-DC
C20:1-OH/C18-DC
C20-OH/C18-DC
C22:3
C22:2
C22:1
C22
C24

Figure S5. MTLN is required for cellular fatty acid metabolism, Related to Figure 5.

(A) Western validation of the physical interaction between endogenous MTLN and CPT1B. Endogenous MTLN was immuno-isolated from mouse hearts.

(B) BN-PAGE analysis of MTLN, CPT1B, HADHA, NDUFA9, and ATP5A using mitochondria isolated from mouse heart.

(C) Western validation of the physical interaction between MTLN and CYB5B. HA-tagged MTLN and FLAG-tagged CYB5B are expressed from HEK293T cells. FLAG-CYB5B served as the bait.

(D) Oxidation of radioactive palmitic acid as measured by the production of ^{14}C labeled CO_2 in skeletal muscle homogenate. Skeletal muscle homogenates were freshly isolated from fed animals.

(E) As in panel C, oxidation of radioactive palmitic acid as measured by the production of acid soluble metabolites (ASM).

(F-G) Similar to Fig.4D and E, heart tissue homogenates were prepared from animals fasted for 12 h and assayed for the oxidation of radioactive palmitic acid in forms of CO_2 and ASM production.

(H-I) Similar to panel E to F, heart homogenates were prepared from fed animals.

(J) Rate of mitochondrial respiration was measured by Seahorse using palmitoyl-carnitine as the substrate. Purified mouse heart mitochondria were used in this assay.

(K) Mouse skeletal muscle acylcarnitine profiles was measured by targeted metabolomics.

(L) Enzymatic activity of CPT1 was measured using purified mouse heart mitochondria.

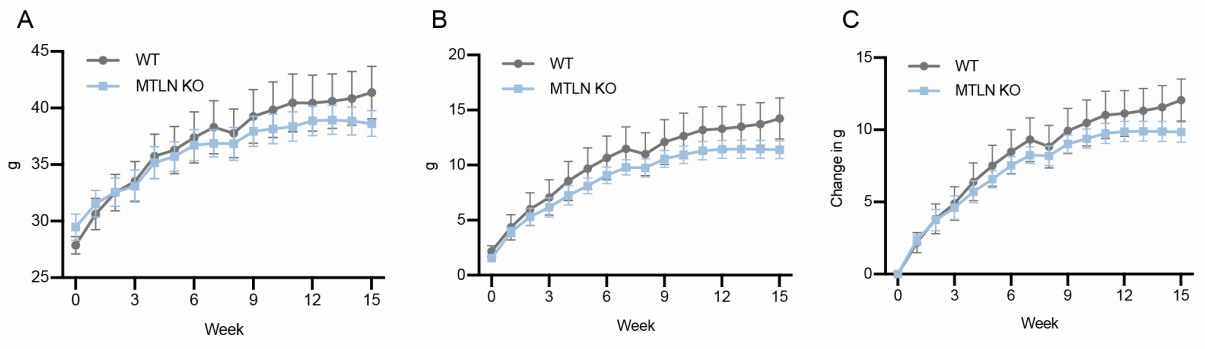

Figure S6. Loss of MTLN protects mouse from diet-induced insulin resistance, Related to Figure 6.

(A) Body weight of animals under the WDF diet in a 16-week feeding.

(B) Body fat mass of animals under WDF diet feeding as determined by quantitative MRI.

(C) Change in body mass of animals under WDF diet feeding as determined by quantitative MRI.